BACKSCATTER FROM A SCALE-SIMILARITY MODEL: EMBEDDED LES OF CHANNEL FLOW, DEVELOPING BOUNDARY LAYER FLOW AND BACKSTEP FLOW

L. Davidson
Department of Applied Mechanics
Chalmers University of Technology
SE-412 96 Gothenburg, Sweden
lada@chalmers.se

ABSTRACT

The scale-similarity model was proposed by Bardina *et al.* (1980) some 30 years ago. It was found not to be sufficiently dissipative. Much later, Davidson (2009) found a way to make it strictly dissipative. This was simply achieved by selecting those instants when the scale-similarity term in the momentum equation has the same sign as the viscous diffusive term (the latter term is indeed dissipative). In Davidson (2009) this technique was also used the other way around: by selecting time instants when the scale-similarity term has the *opposite* sign to the viscous diffusion term it acts as a backscatter term, which destabilizes the momentum equation. This feature is exploited in the present work to promote the generation of resolved turbulence. It is used to promote the creation of resolved turbulence in embedded LES of channel flow, and LES of developing boundary layer and backstep flow. The present method reduces the gray area problem described by Spalart (2009). The proposed method can also be used to promote transition from laminar to turbulent flow.

1 BACKSCATTER FROM THE SCALE-SIMILARITY MODEL

The momentum equations for LES, with a turbulent viscosity and an additional SGS stress tensor, τ_{ik}, from the scale-similarity model, read

$$\frac{D\bar{u}_i}{Dt}+\frac{1}{\rho}\frac{\partial \bar{p}}{\partial x_i}=\frac{\partial}{\partial x_k}\left((\nu+\nu_{SGS})\frac{\partial \bar{u}_i}{\partial x_k}\right)-\left(\frac{\partial \tau_{ik}}{\partial x_k}\right)^{-} \quad (1)$$

where D/Dt denotes material derivative; superscript $'-'$ denotes backscatter. The stress tensor, τ_{ik}, is obtained from the scale-similarity model (Speziale, 1985)

$$\tau_{ik}=\overline{u_i u_k}-\bar{\bar{u}}_i\bar{\bar{u}}_k \quad (2)$$

The explicit filtering in Eq. 2 is carried out on a grid of 2Δ; hence the SGS stress stress can be regarded as a dynamic Leonard stress in the dynamic model (Germano *et al.*, 1991). In the present study $-\partial\tau_{ik}/\partial x_k$ is used as a *forcing* term (i.e. backscatter), see Eq. 1. Hence, we must make sure that it does not give rise to any SGS dissipation (i.e. forward scatter) but only backscatter. To this end, let us take a closer look at the equation for the resolved, turbulent kinetic energy, $K=\langle \bar{u}_i'\bar{u}_i'\rangle/2$, which reads ($\langle . \rangle$ denotes averaging in time)

$$\frac{DK}{Dt}+\langle \bar{u}_k'\bar{u}_i'\rangle\frac{\partial\langle\bar{u}_i\rangle}{\partial x_k}+\frac{1}{\rho}\frac{\partial\langle\bar{p}'\bar{u}_i'\rangle}{\partial x_i}+\frac{1}{2}\frac{\partial\langle\bar{u}_k'\bar{u}_i'\bar{u}_i'\rangle}{\partial x_k}= \nu\left\langle\frac{\partial^2\bar{u}_i'}{\partial x_k\partial x_k}\bar{u}_i'\right\rangle-\left\langle\left(\frac{\partial\tau_{ik}}{\partial x_k}-\left\langle\frac{\partial\tau_{ik}}{\partial x_k}\right\rangle\right)\bar{u}_i'\right\rangle \quad (3)$$

where the right side represents the viscous and SGS diffusion terms in the momentum equation for $\bar{u}_i'$, multiplied by the fluctuating velocity, $\bar{u}_i'$. The right side can be re-written as

$$\underbrace{\nu\left\langle\frac{\partial^2\bar{u}_i'}{\partial x_k\partial x_k}\bar{u}_i'\right\rangle}_{\varepsilon^{non}}-\left\langle\frac{\partial\tau_{ik}}{\partial x_k}\bar{u}_i'\right\rangle= \nu\frac{\partial^2 K}{\partial x_k\partial x_k}-\underbrace{\nu\left\langle\frac{\partial\bar{u}_i'}{\partial x_k}\frac{\partial\bar{u}_i'}{\partial x_k}\right\rangle}_{\varepsilon}-\underbrace{\left\langle\frac{\partial\tau_{ik}}{\partial x_k}\bar{u}_i'\right\rangle}_{\varepsilon_{SGS}} \quad (4)$$

The first term on the left side is the non-isotropic (i.e. the true) viscous dissipation, ε^{non}; this is predominately negative. The first term on the right side is the viscous diffusion, and the second term, ε, is the (isotropic) viscous dissipation, which is always positive. The last term, ε_{SGS}, is a source term arising from the SGS stress tensor, which can be positive or negative. When it is positive, forward scattering takes place (i.e. it acts as a dissipation term); when it is negative, back scattering occurs. Hence, to achieve forcing, we want to make sure that this term is negative.

Consider the left side of Eq. 4. We know that the viscous diffusion in the momentum equation is dissi-

pative (forward scatter in the K equation). We want the SGS stress tensor to act as backscatter in the K equation. Hence we add the SGS stress tensor term, $-\partial\tau_{ik}/\partial x_k$, to the momentum equation only when its sign is *opposite* to that of the viscous diffusion term. This is conveniently achieved as (Davidson, 2009)

$$M_{ik} = \text{sign}\left(\frac{\partial\tau_{ik}}{\partial x_k}\frac{\partial^2\overline{u}_i'}{\partial x_k\partial x_k}\right). \quad (5)$$

(no summation on i,k). The resolved fluctuation, $\overline{u}_i'$, is not known at run-time. It could be computed as $\overline{u}_i' = \overline{u}_i - \langle\overline{u}_i\rangle_{ra}$, where $\langle\overline{u}_i\rangle_{ra}$ denotes the running-time average of $\overline{u}_i$. It was shown in Davidson (2009) that, for $y^+ \gtrsim 20$ in channel flow, the second derivative of $\overline{u}_i'$ is almost 100% correlated with that of $\overline{u}_i$. Hence, in the present work, Eq. 5 is replaced by

$$M_{ik} = \text{sign}\left(\frac{\partial\tau_{ik}}{\partial x_k}\frac{\partial^2\overline{u}_i}{\partial x_k\partial x_k}\right) \quad (6)$$

(no summation on i,k). Each component of the divergence of the SGS stress tensor in Eq. 1 is then simply multiplied by $\tilde{M}_{ik}$, i.e.

$$\tilde{M}_{ik} = \max(M_{ik},0), \quad \left(\frac{\partial\tau_{ik}}{\partial x_k}\right)^- = -\tilde{M}_{ik}\frac{\partial\tau_{ik}}{\partial x_k} \quad (7)$$

(no summation on k). In Davidson (2009), the scale-similarity model was used for forcing in a small, local region surrounding the RANS-LES interface. In the present work, it is used in the entire LES region. Because the role of this term is to act as a forcing term, it may happen that the forcing becomes too large, making the numerical solution of the equation system unstable. Hence the magnitude of the forcing term must be limited. Its magnitude in the present work is limited by relating it to part of the diffusion as

$$\left|-\frac{\partial\tau_{ik}}{\partial x_k}\right| \le \beta(\nu+\nu_{SGS})\left|\frac{\partial^2\overline{u}_i}{\partial x_k\partial x_k}\right|, \text{no summation on } k \quad (8)$$

The baseline value of β is $\beta = 2$.

In the present work, the scale-similarity stresses, Eq. 2, are computed by explicit filtering; an alternative approach may be to estimate them using Leonard expansion (Peng & Davidson, 2009; Peng, 2012).

2 THE PANS LRN $k-\varepsilon$ MODEL

The LRN PANS turbulence model (Girimaji, 2006; Ma *et al.*, 2011) is used and reads

$$\frac{Dk}{Dt} = \frac{\partial}{\partial x_j}\left[\left(\nu+\frac{\nu_t}{\sigma_{ku}}\right)\frac{\partial k}{\partial x_j}\right] + P_k - \varepsilon$$

$$\frac{D\varepsilon}{Dt} = \frac{\partial}{\partial x_j}\left[\left(\nu+\frac{\nu_t}{\sigma_{\varepsilon u}}\right)\frac{\partial\varepsilon}{\partial x_j}\right] + C_{\varepsilon1}P_k\frac{\varepsilon}{k} - C^*_{\varepsilon2}\frac{\varepsilon^2}{k}$$

$$\nu_t = C_\mu f_\mu\frac{k^2}{\varepsilon}, C^*_{\varepsilon2} = C_{\varepsilon1} + \frac{f_k}{f_\varepsilon}(C_{\varepsilon2}f_2 - C_{\varepsilon1})$$

$$\sigma_k \equiv \sigma_k\frac{f_k^2}{f_\varepsilon}, \quad \sigma_{\varepsilon u} \equiv \sigma_\varepsilon\frac{f_k^2}{f_\varepsilon}$$

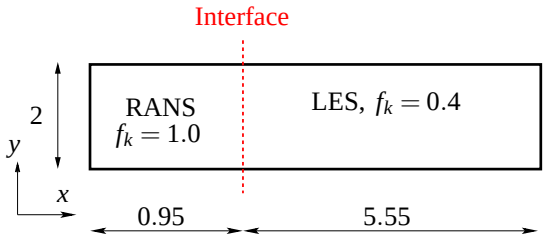

(a) Channel flow. The vertical interface separates the RANS and the LES regions.

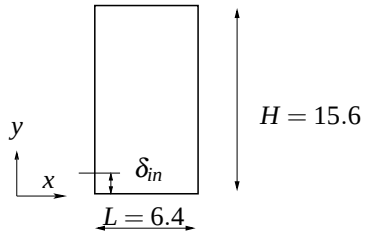

(b) Boundary layer flow. $\delta_{in} = 1$, $Z_{max} = 1.6$

Figure 1. Flow configurations.

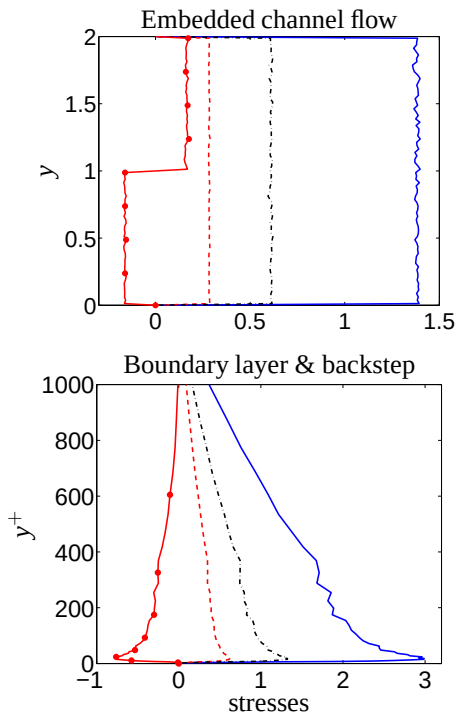

Figure 2. Added synthetic fluctuations at interface or inlet. ——: $\overline{u}'^+_{rms}$; - - -: $\overline{v}'^+_{rms}$; - · -: $\overline{w}'^+_{rms}$; —●—: $\langle\overline{u}'\overline{v}'\rangle^+$.

where $f_\varepsilon = 1$. In the LES region, $f_k = 0.4$.

3 NUMERICAL METHOD

An incompressible, finite volume code is used (Davidson & Peng, 2003). The convective terms

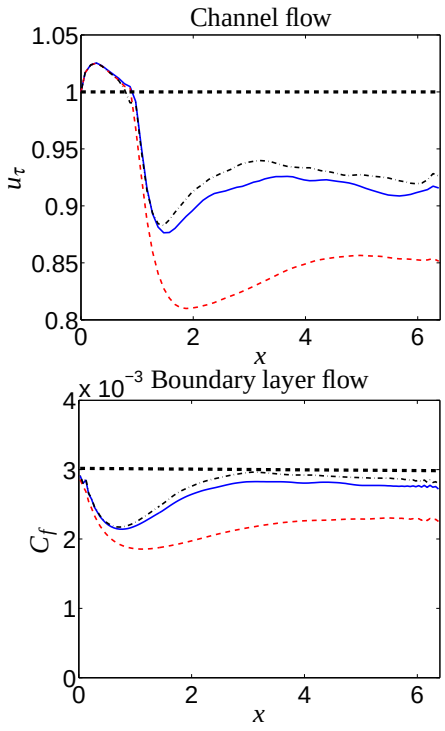

Figure 3. Skin friction. —— backscatter; - - - no backscatter; - - - backscatter with $\beta = 3$, see Eq. 8; ▬ ▬ ▬ :target value.

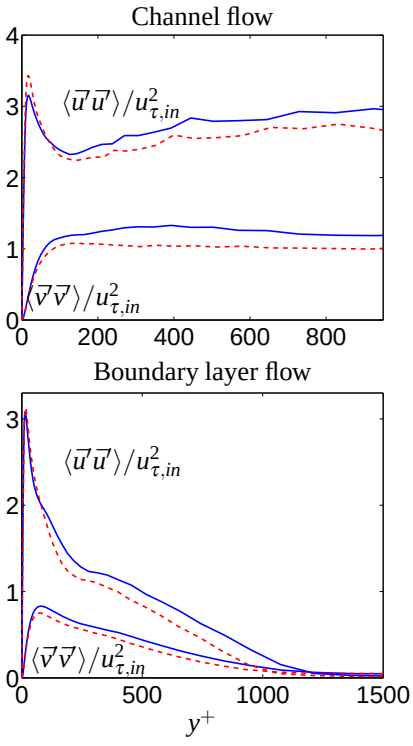

Figure 4. Resolved normal stresses at $x = 3$. —— backscatter; - - - no backscatter.

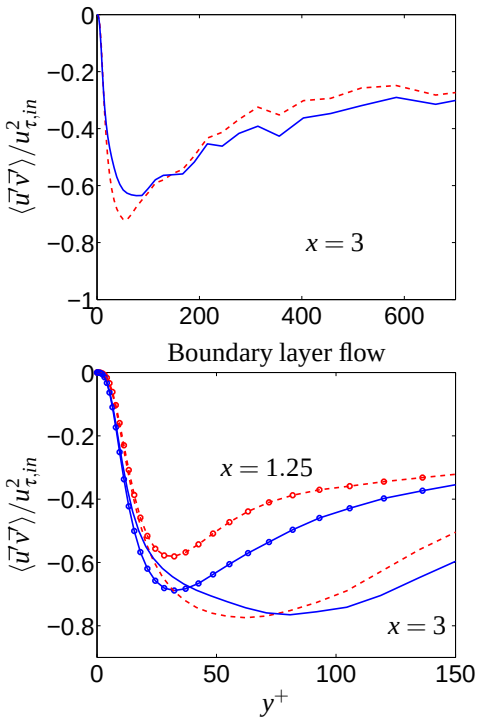

Figure 5. Resolved shear stresses. $x = 1.25$: with markers; $x = 3$: without markers. —— backscatter; - - - no backscatter.

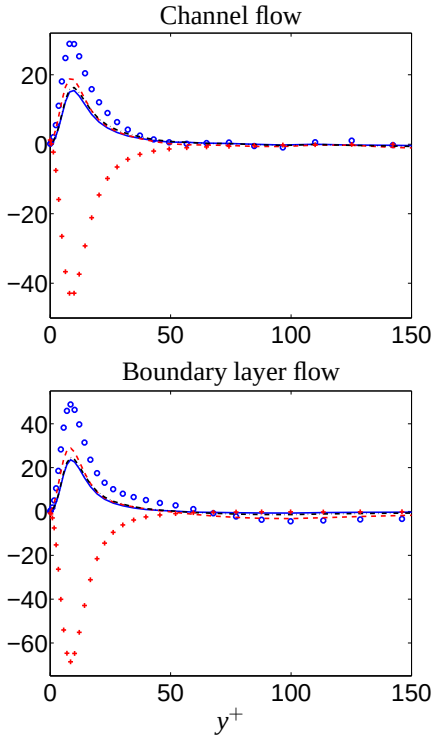

Figure 6. Shear stresses at $x = 3$. —— $\langle(-\partial\tau_{12}/\partial y)^-\rangle$; - - - $\langle-\partial\tau_{12}/\partial y\rangle$, Eq. 8 not used; - - - $\langle(-\partial\tau_{12}/\partial y)^-\rangle$, Eq. 8 not used; ○: $-\partial\langle\overline{u}'\overline{v}'\rangle/\partial y$. +: $\partial/\partial y\langle((\nu+\nu_{SGS})\partial\overline{u}/\partial y)\rangle$.

in the momentum equations are discretized using 95% central differencing and 5% second-order bounded upwinding (van Leer (1974)). The k and ε are discretized using the hybrid scheme (first-order hybrid upwinding and central differencing). The second-

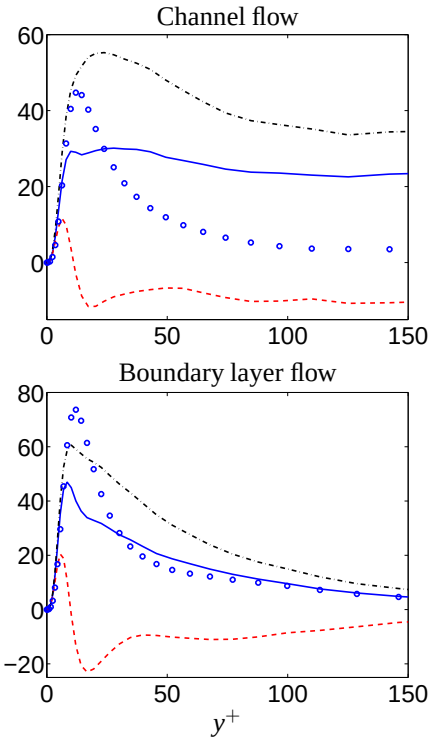

Figure 7. Terms in the K equation, see Eq. 4. —— $-\bar{\varepsilon}_{SGS}$; - - - $-\varepsilon_{SGS}$, Eq. 8 not used; -·-·- $-\bar{\varepsilon}_{SGS}$, Eq. 8 not used; ○: 40% of $\langle -\bar{u}\bar{v}\rangle \partial\langle\bar{u}\rangle/\partial y$.

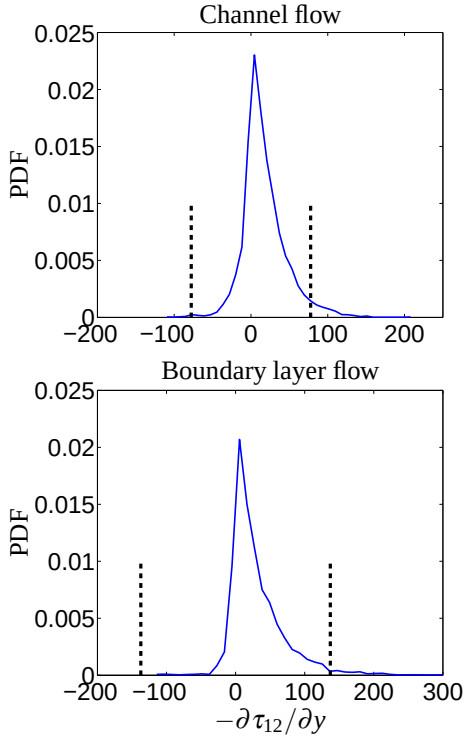

Figure 8. Probability density function (PDF) of $-\partial\tau_{12}/\partial y$, at $x = 2.5$, $y^+ \simeq 10$. Thick vertical dashed lines: $\pm 2\langle(\nu+\nu_t)\partial^2\bar{u}/\partial y^2\rangle$.

order accurate Crank-Nicolson is used in time.

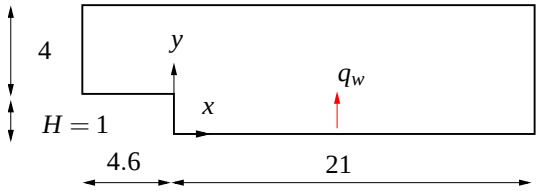

Figure 9. Backstep flow, computational domain.

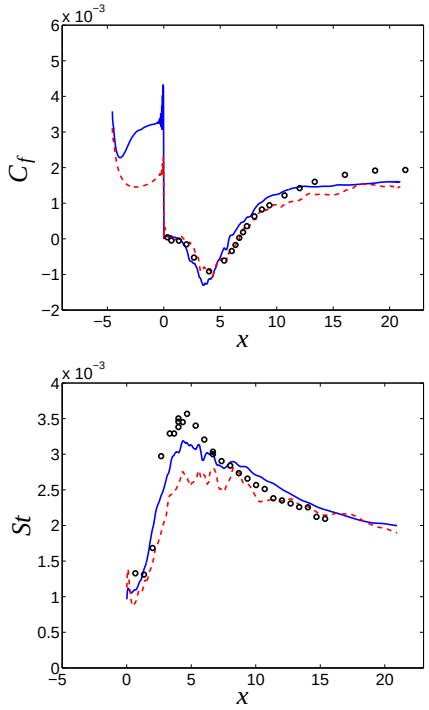

Figure 10. Backstep flow. Skin friction and Stanton number. Experiments Vogel & Eaton (1985). —— backscatter; - - - no backscatter.

4 RESULTS

We present results from three flows, embedded LES in a channel flow, LES of a flat-plate boundary layer and LES of the flow over a backstep. Anisotropic fluctuating velocities (Davidson & Peng, 2013) are used at the interface in the channel flow and at the inlet in the boundary layer flow and the backstep flow, see Fig. 2. It may be noted that the inlet fluctuations are scaled with k_{RANS} (where k_{RANS} comes from a pre-cursor RANS simulations) for the boundary layer and backstep flow, whereas they are not scaled for the channel flow. It was found in Davidson (2007) that, for channel flow, this approach is more efficient in creating resolved turbulence.

4.1 Channel and boundary layer flow

The Reynolds number for the channel flow is $Re_\tau = 950$ based on the friction velocity, u_τ, and half the channel width, δ, see Fig. 1. With a $6.4 \times 2 \times 1.6$ domain, a mesh with $128 \times 80 \times 32$ cells is used in the streamwise (x), the wall-normal (y) and the spanwise (z) direction. Forcing (backscatter) is used in the entire LES region.

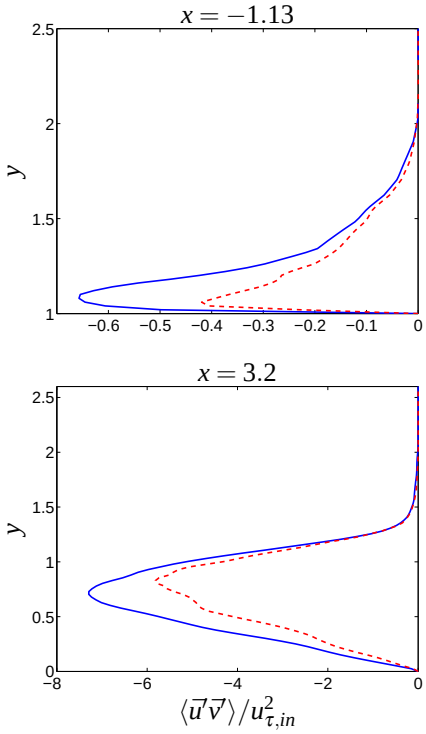

Figure 11. Backstep flow. Resolved shear stresses. —— backscatter; - - - no backscatter.

The inlet Reynolds number of the boundary layer flow is $Re_\theta = 3600$, which corresponds to $Re_\delta = U_{free}\delta_{in}/\nu \simeq 28000$. The inlet mean profile is taken from DNS (Schlatter & Orlu, 2010). The inlet height, δ_{in}, see Fig. 1, is covered by 45 cells. The grid has $128 \times 96 \times 64$ cells in the streamwise (x), wall-normal (y) and spanwise (z) direction. Forcing (backscatter) is used in the entire domain.

The friction velocity and the skin friction in Fig. 3 show that the backscatter makes the flow approach fully developed conditions much faster than without backscatter. Without backscatter, the skin friction in the boundary flow does not reach the target value. For the channel flow, the u_τ does not reach the target value of one (with or without backscatter) because the spanwise resolution is not sufficient.

The influence of the β coefficient in Eq. 8 is evaluated in Fig. 3. It is increased from the baseline value of $\beta = 2$ to $\beta = 3$. As can be seen, it has little effect for both the boundary layer flow and the embedded channel flow. If β is increased further for the channel flow, nonphysical wiggles appear near the interface. For the boundary layer flow, a value of $\beta = 4$ (not shown) gives the same results as $\beta = 3$. The limitation in the forcing term using Eq. 8 is very important for keeping the equation system stable. The forcing has a strong built-in feedback: the more resolved turbulence that is created with Eqs. 1, 6 and 7, the larger the velocity gradients, and hence the forcing term, $-\partial\tau_{ik}/\partial x_k$, in Eq. 1 is further increased.

The resolved normal and shear stresses are presented in Figs. 4 and 5; it can be seen that the backscatter, as intended, creates additional resolved turbulence. It can also be seen that, in a region close to the wall, the resolved shear stress is larger without backscatter than with backscatter; the reason is probably the dominance of the production term (see Fig. 7).

Figures 6 and 7 show the influence of the backscatter in greater detail. Figure 6 shows the effect in the momentum equation. It can first be noted that the forcing scale-similarity term is fairly large; its magnitude is approximately half of that of the resolved shear stress near the wall ($y^+ \lesssim 20$). The limiter in Eq. 7 is active (i.e. $\tilde{M}_{ik} = 1$) during approximately 50% of the time for $y^+ > 30$ and is even more often active near the wall (maximum value of 80% at $y^+ \simeq 10$). This means that at the time instants when the term $-\partial\tau_{ik}/\partial x_k$ acts as backscatter, it is actually twice as large (even larger near the wall) than what is shown in Fig. 6, see also Fig. 8. The limiter in Eq. 8 is much less active: it is active for less than 10% at all y locations. Thus the forcing scale-similarity terms in Fig. 6 with and without the limiter in Eq. 8 are virtually identical. It should be mentioned that all results presented in Figs. 6 and 7 were obtained with Eqs. 7 and 8 active; they are made inactive only in the post-processing.

The contribution of the forcing scale-similarity term to the resolved kinetic energy, K (see Eqs. 3 and 4), is shown in Fig. 7. As in the momentum equation, the magnitude of the forcing scale-similarity term is comparable to that of the resolved turbulence (i.e. the production term, $\langle -\overline{u}'\overline{v}'\partial\overline{u}/\partial y \rangle$). The effect of selecting the forcing instants (i.e. ε_{SGS}^-, see Eq. 7) is large. The scale-similarity term itself, ε_{SGS} (i.e. no Eq. 7), is actually dissipative (i.e. $-\varepsilon_{SGS} < 0$) for $y^+ \gtrsim 20$. The limit in Eq. 8 also has a fairly large effect, but the other way around: it limits – as intended – the forcing effect of the scale-similarity term. Without this limit, the equation system rapidly diverges.

Figure 8 presents a histogram of the scale-similarity term at $y^+ \simeq 10$. The limit in Eq. 8 (with $\beta = 2$) is shown as thick vertical dashed lines. As can be seen, the limiter eliminates only extreme instants. In the boundary layer flow, the limit is actually not active for negative $-\partial\tau_{12}/\partial y$. This explains why larger β can be used in the boundary layer flow than in the channel flow. Note that the instantaneous values of the the scale-similarity term (up to 200 and 300 for the boundary layer flow and the channel flow, respectively) are much larger than their mean value (approximately 20 for both flows, see Eq. 6).

4.2 Backstep flow

The Reynolds number for the backstep flow is $Re_H = 28000$, and the experiments were carried out by Vogel & Eaton (1985). The grid has $336 \times 152 \times 64$ cells in the streamwise (x), wall-normal (y) and spanwise (z) directions (see Fig. 9). The step is covered by 96×52 cells in the streamwise and wall-normal directions. The inlet boundary layers at the upper wall and the step are covered by 45 cells; the grid is stretched by 1.12 for $1 < y < 3$ (the same as

for $y < 2$ in the boundary layer simulations). The grid above the step is symmetric around $y = 3$. A constant grid spacing is used in the x direction in $-4.6 < x < -0.27$ with $\Delta x \simeq 0.05$ (the same as in the boundary layer simulations); the grid is geometrically compressed by 0.89 in the region $-0.27 < x < 0$. The extent of the domain in the spanwise direction is 1.6. The mesh in the recirculation region is taken from Shur *et al.* (2008).

The inlet mean profile is taken from DNS (Schlatter & Orlu, 2010) (the same as in the boundary layer simulations). For the temperature, the inlet profile is $t = 0$ (constant in both space and time). At the lower wall, at $y = 0$, a constant heat flux, q_w, is used for $x > 0$. The inlet bulk velocity and H are set to one, so that $\nu = 1/Re_H$. The forcing term in Eq. 1 is used for $x < 1$, $1 < y < 5$. The predictions were not altered to any great extent when the forcing term was used for $x < 7$ (not shown).

The skin friction and the Stanton number are presented in Fig. 10. As can be seen, the skin friction on the step is much better predicted with backscatter in the same way as in the boundary layer flow (see Fig. 3); indeed, the boundary layer on the step is identical to the boundary layer in Section 4.1 (same grid, same inlet boundary conditions). In the recirculation region, the backscatter has no noticeable effect on the skin friction. However, the backscatter does have a noticeable effect on the heat transfer (Stanton number), see Fig. 10. The peak in St is well captured with forcing.

Figure 11 presents the resolved shear stresses on the step and in the recirculation region. As for the channel flow and the boundary layer flow, backscatter increases the resolved turbulence. The influence of backscatter in the boundary layer on the step (Fig. 11) is much larger than in the boundary layer (Fig. 5). The reason may be that, in the backstep flow, the unstable shear layer that emanates at $x = 0$ also introduces fluctuations for $x < 0$, and these fluctuations are enhanced by the forcing backscatter.

5 CONCLUSIONS

The present forcing method was used in embedded LES. One problem in embedded LES is that the flow does not go into turbulence-resolving mode sufficiently quickly. This has been called the *gray area* problem (Spalart, 2009). The present method can be used in the interface region between RANS and LES in general, both in embedded LES (interface normal to the streamwise direction) and zonal hybrid LES-RANS (interface parallel to a wall). The proposed method can also be used to promote transition from laminar to turbulent flow.

The forcing is taken from the scale-similarity model. It is defined as forcing when the sign of the force (per unit volume) from the scale-similarity model is opposite to that of the viscous diffusion. The forcing term could maybe instead be taken from synthetic turbulence or white noise, selecting – as in the present method – the time instants when the force represents backscatter.

REFERENCES

Bardina, J., Ferziger, J.H. & Reynolds, W.C. 1980 Improved subgrid scale models for large eddy simulation. AIAA 80-1357, Snomass, Colorado.

Davidson, L. 2007 Using isotropic synthetic fluctuations as inlet boundary conditions for unsteady simulations. *Adv. and Appl. in Fluid Mech.* **1** (1), 1–35.

Davidson, L. 2009 Hybrid LES-RANS: back scatter from a scale-similarity model used as forcing. *Phil. Trans. Roy. Soc. A* **367** (1899), 2905–2915.

Davidson, L. & Peng, S.-H. 2003 Hybrid LES-RANS: A one-equation SGS model combined with a $k-\omega$ model for predicting recirculating flows. *Int. J. for Num. Methods in Fluids* **43**, 1003–1018.

Davidson, L. & Peng, S.-H. 2013 Embedded large-eddy simulation using the partially averaged Navier-Stokes model. *AIAA J.* **51** (5), 1066–1079.

Germano, M., Piomelli, U., Moin, P. & Cabot, W.H. 1991 A dynamic subgrid-scale eddy viscosity model. *Phys. Fluids A* **3**, 1760–1765.

Girimaji, S.S. 2006 Partially-averaged Navier-Stokes model for turbulence: A Reynolds-averaged Navier-Stokes to direct numerical simulation bridging method. *ASME J. Appl. Mech.* **73** (2), 413–421.

van Leer, B. 1974 Towards the ultimate conservative difference scheme. Monotonicity and conservation combined in a second order scheme. *J. Comp. Phys.* **14** (4), 361–370.

Ma, J., Peng, S.-H., Davidson, L. & Wang, F. 2011 A low Reynolds number variant of Partially-Averaged Navier-Stokes model for turbulence. *Int. J. Heat and Fluid Flow* **32** (3), 652–669.

Peng, S.-H. 2012 Hybrid RANS-LES modelling with an energy backscatter function incorporated in the LES mode. *THMT'12*. Palermo, Sicily/Italy.

Peng, S.-H. & Davidson, L. 2009 Approximation of subgrid-scale stresses based on the Leonard expansion. In *THMT'09*. Rome. Italy.

Schlatter, P. & Orlu, R. 2010 Assessment of direct numerical simulation data of turbulent boundary layers. *J. Fluid Mech.* **659**, 116–126.

Shur, M. L., Spalart, P.R., Strelets, M. Kh. & Travin, A.K. 2008 A hybrid RANS-LES approach with delayed-DES and wall-modelled LES capabilities. *Int. J. Heat and Fluid Flow* **29**, 1638–1649.

Spalart, P.R. 2009 Detached-eddy simulation. *Ann. Rev. Fluid Mech.* **41**, 181–202.

Speziale, C.G. 1985 Galilean invariance of subgrid-scale stress models in the large-eddy simulation of turbulence. *J. Fluid Mech.* **156**, 55–62.

Vogel, J.C. & Eaton, J.K. 1985 Combined heat transfer and fluid dynamic measurements downstream a backward-facing step. *J. Heat Transfer* **107**, 922–929.